ACTA GEOGRAPHICA SLOVENICA

GEOGRAFSKI ZBORNIK

2022
62
3

ACTA GEOGRAPHICA SLOVENICA
GEOGRAFSKI ZBORNIK
62-3 • 2022

Contents

Aida AVDIĆ, Boris AVDIĆ, Ivan ZUPANC
Socio-demographic analysis of border regions of Bosnia and Herzegovina 7

Erika DŽAJIĆ URŠIČ, Igor JELEN
From industrial district to industrial symbiosis: An opportunity. The case of the Ponte Rosso industrial area, Italy 21

Tamara BOŽOVIĆ, Miroslav D. VUJIČIĆ, Sanja KOVAČIĆ, Tamara JOVANOVIĆ, Tatjana PIVAC
Tourist motivation for slow travel: A case study of the Vojvodina Region, Serbia 33

Entin HIDAYAH, Tedy PRANADIARSO, Gusfan HALIK, Indarto INDARTO, Wei-Koon LEE, Mokhammad Farid MARUF
Flood mapping based on open-source remote sensing data using an efficient band combination system 47

Vanya STAMENOVA, Stefan STAMENOV
Integrated method for global land cover products' validation on the example of Bulgaria 63

Matjaž GERŠIČ, Primož GAŠPERIČ, Petra RUS, Mateja ŠMID HRIBAR, Nika RAZPOTNIK VISKOVIĆ
Sustainable certification of a tourist destination through the prism of visitor's point of view 85

ISSN 1581-6613

ACTA GEOGRAPHICA SLOVENICA

62-3
2022

ISSN: 1581-6613
UDC: 91
2022, ZRC SAZU, Geografski inštitut Antona Melika

Issued by/izdajatelj: Geografski inštitut Antona Melika ZRC SAZU
Published by/založnik: Založba ZRC
Co-published by/sozaložnik: Slovenska akademija znanosti in umetnosti

Address/naslov: Geografski inštitut Antona Melika ZRC SAZU, Gosposka ulica 13, p. p. 306, SI – 1000 Ljubljana, Slovenija; ags@zrc-sazu.si

The articles are available on-line/prispevki so dostopni na medmrežju: http://ags.zrc-sazu.si (ISSN: 1581–8314)

Ordering/naročanje: Založba ZRC, Novi trg 2, p. p. 306, SI – 1001 Ljubljana, Slovenija; zalozba@zrc-sazu.si

Annual subscription/letna naročnina: 20 € for individuals/za posameznike, 28 € for institutions/za ustanove
Single issue/cena posamezne številke: 12,50 € for individuals/za posameznike, 16 € for institutions/za ustanove

Cartography/kartografija: Geografski inštitut Antona Melika ZRC SAZU
Translations/prevodi: DEKS, d. o. o.
DTP/prelom: SYNCOMP, d. o. o.
Printed by/tiskarna: Birografika Bori
Print run/naklada: 400 copies/izvodov

The journal is subsidized by the Slovenian Research Agency and is issued in the framework of the Geography of Slovenia core research programme (P6-0101)/Revija izhaja s podporo Javne agencije za raziskovalno dejavnost Republike Slovenije in nastaja v okviru raziskovalnega programa Geografija Slovenije (P6-0101).

The journal is indexed also in/revija je vključena tudi v: Clarivate Web of Science (SCIE – Science Citation Index Expanded; JCR – Journal Citation Report/Science Edition), Scopus, ERIH PLUS, GEOBASE Journals, Current geographical publications, EBSCOhost, Georef, FRANCIS, SJR (SCImago Journal & Country Rank), OCLC WorldCat, Google scholar, CrossRef, and DOAJ.

Design by/Oblikovanje: Matjaž Vipotnik

Front cover photography: The Temple of Concordia (Agrigento, Italy) is one of the best preserved in the Valley of the Temples and resembles the logo of the international organization UNESCO. Cultural and natural heritage sites are often the focus of various research disciplines (photograph: Rok Ciglič).
Fotografija na naslovnici: Tempelj enotnosti (Agrigento, Italija) je eden izmed bolj ohranjenih v Dolini templjev in spominja na logotip mednarodne organizacije UNESCO. Kulturna in naravna dediščina sta pogosto v ospredju različnih raziskovalnih disciplin (fotografija: Rok Ciglič).

Acta geographica Slovenica, 62-3, 2022, 47–62

FLOOD MAPPING BASED ON OPEN-SOURCE REMOTE SENSING DATA USING AN EFFICIENT BAND COMBINATION SYSTEM

Entin Hidayah, Tedy Pranadiarso, Gusfan Halik, Indarto Indarto,
Wei-Koon Lee, Mokhammad Farid Maruf

ANGGER PUTRANTO

Flooding in the Tempurejo sub-district, Jember Regency, East Java Province, Indonesia.

DOI: https://doi.org/10.3986/AGS.10598
UDC: 528:566.166(594)
COBISS: 1.01

Entin Hidayah[1], Tedy Pranadiarso[1], Gusfan Halik[1], Indarto Indarto[2], Wei-Koon Lee[3], Mokhammad Farid Maruf[1]

Flood mapping based on open-source remote sensing data using an efficient band combination system

ABSTRACT: Flood mapping is an essential component of planning flood mitigation. The availability of remote sensing data makes rapid flood mapping possible. This article develops an accurate method for rapid flood mapping using satellite imagery. Sentinel-2 imagery was tested by acquiring data before and after a flood event in a lowland area. Flooding extraction was performed using the newly developed Flood Inundation Extraction Index (FIEI) and compared to the Modified Normalized Difference Water Index (MNDWI), the most commonly used index. Based on the choice of threshold, the results are divided into flooded and non-flooded areas. Evaluation of the performance accuracy based on the total and kappa coefficients showed that the FIEI approach is more accurate than the MNDWI approach.

KEY WORDS: rapid flood mapping, Sentinel-2, Modified Normalized Difference Water Index, Flood Inundation Extraction Index, kappa coefficient, accuracy, Indonesia

Kartiranje poplav na podlagi odprtokodnih podatkov daljinskega zaznavanja z učinkovitim sistemom kombiniranih pasov

POVZETEK: Kartiranje poplav je ključno za načrtovanje blažitev njihovih posledic. Razpoložljivi podatki, zajeti z daljinskim zaznavanjem, nam to omogočajo. V članku razvijamo natančno metodo za hitro kartiranje poplav na podlagi satelitskih posnetkov. Posnetke Sentinel-2 smo testirali s podatki pred in po poplavi v nižinskem območju. Poplave smo zaznavali s pomočjo na novo razvitega ekstrakcijskega indeksa najvišjih poplav (FIEI) in ga primerjali s prilagojenim normaliziranim vodnim indeksom (MNDWI), ki je najpogosteje uporabljen indeks v tovrstnih raziskavah. Območja smo glede na izbor določenega praga razdelili na poplavljena in nepoplavljena. Vrednotenje natančnosti rezultatov na podlagi skupnih in kapa koeficientov je pokazalo, da je pristop FIEI natančnejši od pristopa MNDWI.

KLJUČNE BESEDE: hitro kartiranje poplav, Sentinel-2, prilagojen normalizirani vodni indeks, ekstrakcijski indeks najvišjih poplav, kapa koeficient, pravilnost, Indonezija

The article was submitted for publication on 25th February, 2022.
Uredništvo je prejelo prispevek 25. februarja 2022.

[1] University of Jember, Faculty of Engineering, Department of Civil Engineering, Jember, Indonesia
entin.teknik@unej.ac.id (https://orcid.org/0000-0002-1233-6850), tedyteknik@gmail.com (https://orcid.org/0000-0003-2740-848X), gusfan.teknik@unej.ac.id (https://orcid.org/0000-0002-5447-1268), farid.teknik@unej.ac.id (https://orcid.org/0000-0002-5715-935X)

[2] University of Jember, Faculty of Agricultural Technology, Department of Agricultural Engineering, Jember, Indonesia
indarto.ftp@unej.ac.id (https://orcid.org/0000-0001-6319-6731)

[3] University Teknologi Mara, School of Civil Engineering, Shah Alam, Malaysia
leewei994@uitm.edu.my (https://orcid.org/0000-0003-3910-4870)

1 Introduction

A flood is a natural disaster in which a place is inundated for a specific duration, leading to damage to property and loss of life (Huang and Jin 2020; Mahmood et al. 2021). Floods occur due to heavy rainfall, which increases basin runoff, causing the water levels in municipal drainage, water bodies, and rivers to overflow beyond their capacity (Gašparovič and Klobučar 2021). Accurate mapping of flooded areas is a critical step in flood mitigation. However, the conventional approach to predicting flooded areas takes a long time and cannot provide timely information during disasters (Ferk et al. 2021). Moreover, traditional land observation methods are expensive and time-consuming (Rahman et al. 2019).

Flood mapping can provide near real-time data and readily accessible information to predict flooded areas (Sivanpillai et al. 2021). Satellite remote-sensing technology may provide fast information on flood maps (Chen et al. 2019). Furthermore, the integration of remote sensing data and geographic information systems (GIS) has been developed to map flooded areas (Wang et al. 2002). The integrated method of water body mapping is based on indices and mapping flooded areas (Sarp and Ozcelik 2017; Zhou et al. 2017). The approach has created opportunities for quantitative analysis of disaster events across all geographic and spatial scales, including flood mapping. Remote-sensing technology has been developed to provide fast information needed to produce near real-time predictions of flood maps (Sajjad et al. 2022). The technology makes possible quick action by emergency response agencies during a flood event (Sivanpillai et al. 2021).

Previously, Feyisa et al. (2014) used Landsat TM5 images to compare the Automated Water Extraction Index (AWEI), maximum likelihood (ML), Normalized Difference Water Index (NDWI), and Modified NDWI (MNDWI) methods. These methods were applied to five research locations with varying threshold values (TVs) for each site. The AWEI method showed greater accuracy than NDWI, MNDWI, and ML. Another study attempted to combine synthetic aperture radar (SAR) Sentinel-1 and Sentinel-2 imagery data using the NDWI method to quickly and cheaply predict flooding (Huang and Jin 2020). Fisher et al. (2016) used several indices from Landsat TM, ETM+, and OLI images for mapping flooded areas using the water index (WI). The results showed that the WI_{2015}, WI_{2006}, and $AWEI_{shadow}$ methods had the best accuracy. The kappa and overall coefficients reached 95% to 99%. Sivanpillai et al. (2021) recommended the MNDWI method for predicting flooded areas and also to validate the maps by exploring spectral bands 3 and 12 of Sentinel-2. In addition, the MNDWI method was successfully applied to water areas with a background dominated by built-up land (Sivanpillai et al. 2021).

Flood mapping for complex land cover requires sensitive spectral combinations to detect floods in lowland areas. Niwas et al. (2015) and Ettehadi Osgouei et al. (2019) explained that near-infrared (NIR) waves are suitable for detecting water, and green waves are best for detecting vegetation areas. Mid-infrared (MIR) waves are suitable for detecting open land or built-up areas. Remote sensing technology for rapid flood mapping is needed to determine evacuation priorities and mitigation in flood events. Flooded areas can be extracted on the basis of a certain TV of a selected index. However, each image extracted in several locations has a TV that varies according to the location and time of image acquisition, affecting the resulting accuracy (Feyisa et al. 2014). This indicates a development gap for further research to ensure that the correct TV is adopted for the specific geographical region, image type, and date. Therefore, a new approach is needed to flood mapping with complex land cover. Previous studies using Landsat imagery with the NDWI and MNDWI approach in the Citarum watershed, the Bengawan Solo watershed, and the lowland area of Purworejo, Indonesia, have not yielded satisfactory results (Suwarsono et al. 2013).

Based on the spectral bands used in NDWI and MDWI, this study aims to improve the accuracy by modifying spectral combinations and testing flood thresholds using Sentinel-2 image data. The Flood Inundation Extraction Index (FIEI) approach has been developed to distinguish between flooded and non-flooded areas using a suitable TV for application in multiple locations. The rapid flood mapping developed using remote sensing integrated with GIS aims to determine priorities for handling flood-affected areas.

2 The study area

The study area covers the Tempurejo sub-district (524.46 km^2) in the southern part of Jember Regency, East Java Province, Indonesia. According to the National Disaster Management Agency, flood events in the sub-district often occur at the beginning of the year and repeat annually (https://gis.bnpb.go.id/). The

five flood-prone areas included in the study are the villages of Curahnongko, Curahtakir, Sidodadi, Sanenrejo, and Wonoasri (Figure 1).

On Friday, February 6th, 2021, the five villages in the sub-district experienced one of the most significant floods of the year. This was caused by high-intensity rainfall for three consecutive days starting on 4th February, 2021, with the Tempurejo rain gauge recording 58 mm, 53 mm, and 90 mm. During the event, the discharge of the Sanenrejo and Curahnongko rivers increased dramatically and overflowed into the residential settlements. The flood depth reached two meters and lasted about four to six days. Around 12,000 houses were flooded, seven worship facilities were damaged, and five educational facilities were severely affected.

3 Methods

The image treatment consists of pre-processing, processing, and post-processing. The pre-processing focuses on data collected from the national flood inventory, European Space Agency Sentinel-2 imagery, and digital elevation model (DEM). Sentinel-2 image data were selected before and after the flood event to describe the flooded area. This study uses a National Digital Elevation Model (DEMNAS) at 8.1 m pixel resolution. The DEM is used for watershed delineation. The processing includes overlay, cropping, indices calculation, flooded area extraction, and TV treatment. If an overall accuracy is less than 75% the accuracy has not reached the best model. To reach the best model, it is necessary to re-treat the TV by changing the TV treatment. Meanwhile, post-processing involves accuracy assessment and model analysis to derive the flood map based on the best model, as summarized in the flowchart in Figure 2.

The new method was applied and tested in five villages, and the success rate was assessed using the overall accuracy, kappa coefficients, user accuracy, and producer accuracy. The performance was benchmarked and compared against the MNDWI method, which is reported to have high accuracy in rapid flood mapping (see Section 1).

3.1 Data collection

Table 1 lists the data types used, including the source and function. The flood inventory used for model validation consists of an in-situ field survey and flood data from the Indonesian National Board for Disaster Management (Indonesian: *Badan Nasional Penanggulangan Bencana*, BNPB) website and the social media (Official Instagram @bpbd_kab.jember) around the Jember Regency Disaster Management Board and the newspaper *Akurat.co* (Nurullatifah 2021).

Flood extraction was performed using the Sentinel-2 imagery taken before and after February 5th, 2021. The corresponding satellite images used are January 21st, 2020, and February 9th, 2021, corresponding to before and after the flood event. The flood event inventory data were taken in the field, which excludes permanent water areas. The Sentinel-2 image data used are data before and after the flood incident to compare the flood before and after the incident and determine the flooded area. Pre-flood data are used to determine the location of permanent water bodies. Post-flood data describe the entire site of the flood. The administrative boundary and DEMNAS data were obtained from the Indonesian Geospatial Information Agency (Indonesian: *Badan Informasi Geospasial*, BIG). In addition, the DEM data use the vertical datum EGM2008 with a root mean square error (RMSE) value of 2.79 m and a standard error value of −0.13 m.

3.2 Spectral bands

Table 2 shows the four spectral bands of Sentinel-2 datasets, including the wavelength, spatial resolution, and principal applications (SUHET 2015; Niwas et al. 2015; Bousbih et al. 2019).

Past research using the NDWI (Sentinel-2 bands 3 and 8) and the MNDWI (bands 3 and 12) reported that, for pixel values ranging from −1 to 1, values from 0 to 1 best represent open water (i.e., flooding;

Figure 1: The study area. ➤ p. 51

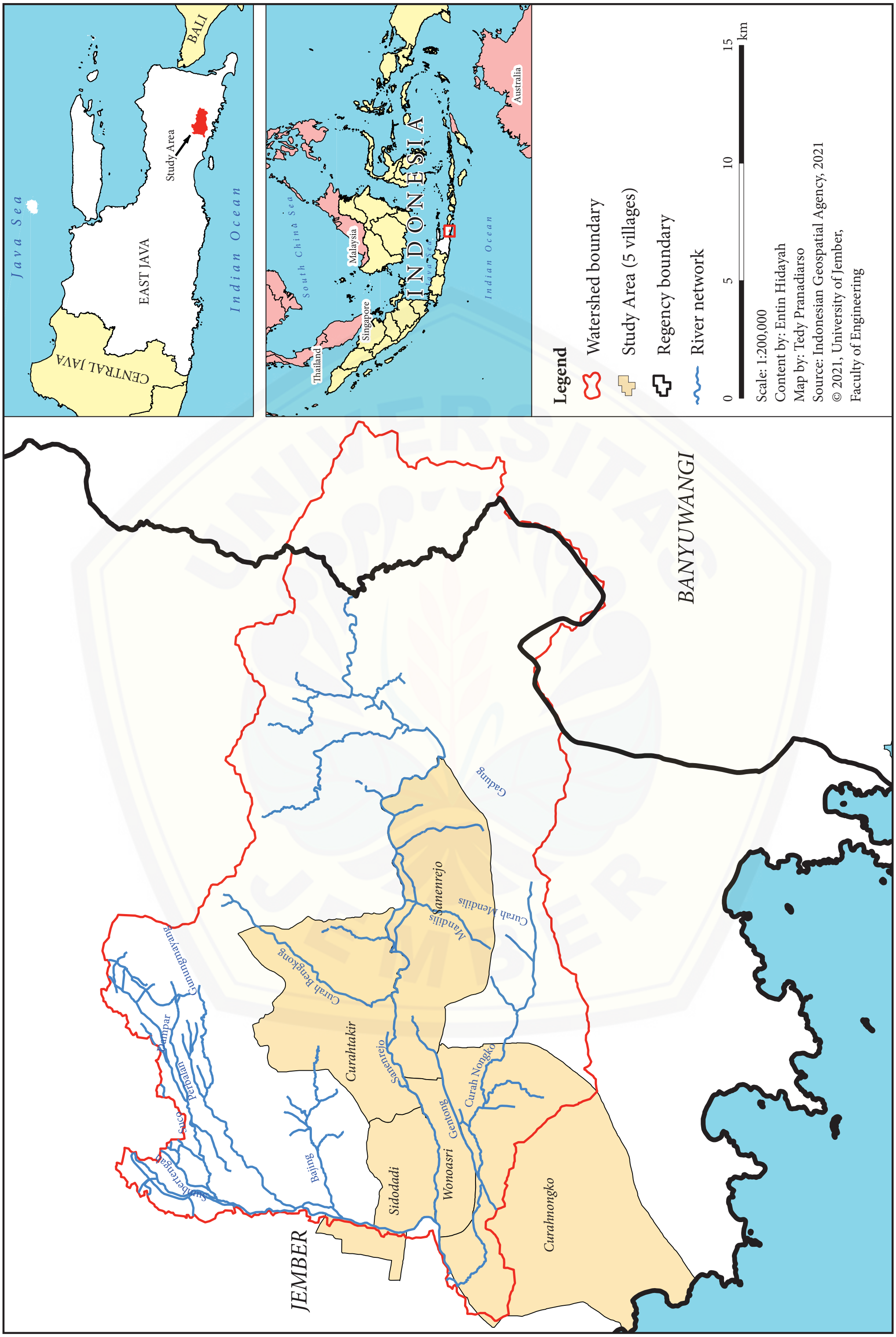

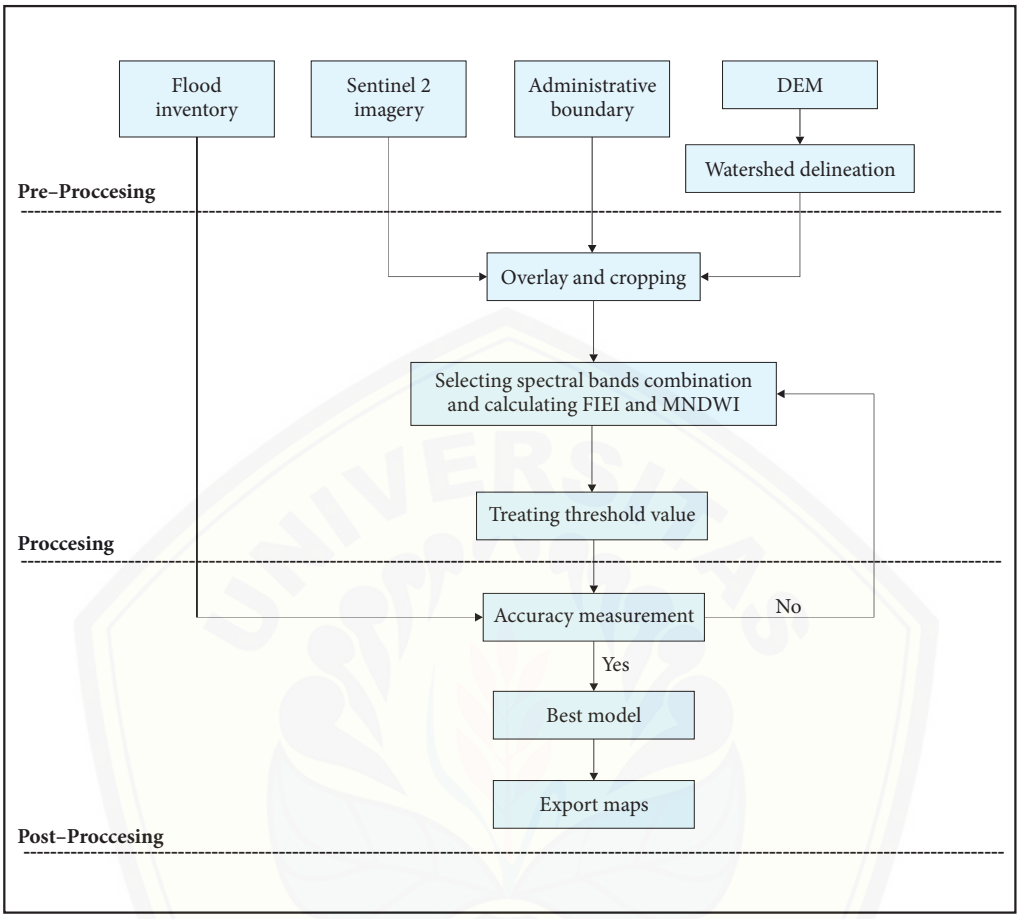

Figure 2: Three-stage methodology flowchart.

Table 1: Data sources.

No.	Data type	Source	Function
1	Flood inventory	• Field survey • Indonesian National Board for Disaster Management (www.gis.bnpb.go.id) • Jember Disaster Management Board (Instagram @BPBD Jember Regency)	Validation of model results
2	Citra Sentinel 2-L1C imagery	Sentinels Scientific Data Hub (https://scihub.copernicus.eu/)	Flooding extraction
3	Administrative boundary	Indonesian Geospatial Information Agency (BIG) (https://tanahair.indonesia.go.id, https://geoservices.big.go.id)	Boundary of villages
4	Digital elevation model (DEM) (resolution = 8.1 × 8.1 m)	Indonesian Geospatial Information Agency (BIG) (https://tanahair.indonesia.go.id)	Delineation of watershed (boundary of study) and river network system

Table 2: Spectral bands of Sentinel-2 L1C imagery (Niwas et al. 2015; SUHET 2015; Bousbih et al. 2019).

No.	Spectral band	Wavelength (nm)	Spatial resolution (m)	Principal applications
1	B03–Green	560	10	Green reflectance by healthy vegetation
2	B08–NIR	842	10	Biomass surveys, water body delineation
3	B11–MIR	1610	20	Vegetation moisture measurement and built-up
4	B12–MIR	2190	20	Hydrothermal mapping, built-up

Xu 2006). However, the soil and terrestrial vegetation properties have a negative value because NIR and MIR reflectance are higher than green. Niwas et al. (2015) and Ettehadi Osgouei et al. (2019) explained that NIR and green waves are suitable for detecting water and vegetation areas. In contrast, MIR waves are suitable for detecting open land or built-up areas. Developing a flood mapping method is necessary by combining the green, NIR, and MIR spectral algorithms available in Sentinel-2 satellite imagery. The algorithm was applied to flood mapping with varied land cover such as vegetation, built-up land, and open water, which requires additional sensitivity to detect water and obtain more accurate mapping.

3.3 The Flood Inundation Extraction Index

The FIEI approach with a combination of Sentinel-2 bands 3, 8, and 11 were expected to provide better results in rapid flood mapping. The combinations were assumed to differentiate the best particular land uses in the study area. The process of flooding extraction and mapping was performed using ArcMap 10.8.2 software.

The new formula can be expressed as:

$$FIEI = \frac{B3 - B8 + B11}{B3 + B8 + B11} \quad (1)$$

It uses the spectral reflectance pattern of three land cover types: vegetation, water, and built-up areas. The FIEI will minimize the ratio of the spectral components of bands 3 (green), 8 (NIR), and 11 (MIR). The results of the FIEI approach were evaluated using the Modified Normalized Difference Water Index (MNDWI; Xu 2006).

3.4 The Modified Normalized Difference Water Index

Development of the MNDWI for flood mapping was motivated by research showing that the reflection of NIR waves is suitable for detecting water (e.g., Niwas et al. 2015; Ettehadi Osgouei et al. 2019). Meanwhile, the MNDWI uses green (band 3) and MIR (band 12) to enhance open water features. In MNDWI, the MIR band is used instead of the NIR band. This approach can distinguish between open land and built-up area features frequently correlated with open water.

The MNDWI can be calculated as:

$$MNDWI = \frac{B3 - B12}{B3 + B12} \quad (2)$$

This yields the following results:

1. At MNDWI, water has a positive value because water can absorb more MIR light than NIR;
2. The built-up area has a negative value; and
3. Soil and vegetation have negative values because soil reflects more MIR light than NIR light, and vegetation reflects more MIR light than green light (Xu 2006; Sathianarayanan 2018).

Several studies using the MNDWI approach have shown high accuracy for mapping flooded areas, with an overall accuracy value of 98% to 99% and kappa coefficients of 0.8 to 0.9 (Fisher et al. 2016; Zhou et al. 2017; Sivanpillai et al. 2021).

3.5 Threshold value treatment

According to Feyisa et al. (2014), the pixel TV for extraction of water bodies or flooding varies according to the location and time of image acquisition. In setting the TV of the FIEI, it is necessary to examine the pixel value in detail to ensure greater accuracy of the final result of flood mapping. The TV treatment used in this study is described in Table 3.

Table 3: Threshold value treatment.

No.	Threshold value	Pixel value	Description
1	TV1	< 0	Not flooded
		≥ 0	Flooded
2	TV2	< 0.05	Not flooded
		≥ 0.05	Flooded
3	TV3	< 0.1	Not flooded
		≥ 0.1	Flooded

3.6 Accuracy measurement

The results of the flood mapping from the Sentinel-2 Level 1C satellite imagery using the FIEI and MNDWI were tested for accuracy. For this purpose, ground truth data acquired by field survey were used (328 sites). The flood model performance was evaluated using the following criteria:

$$\text{User accuracy} = \frac{X_{ij}}{X_{i+}} \times 100\% \quad (3)$$

$$\text{Producer accuracy} = \frac{X_{ij}}{X_{+j}} \times 100\% \quad (4)$$

$$\text{Overall accuracy} = \frac{1}{N}\sum_{i=1}^{r} X_{ii} \times 100\% \quad (5)$$

$$\kappa = \frac{N\sum_{i=1}^{r} X_{ii} - \sum_{i=1}^{r} X_{i+} + X_{+i}}{N^2 - \sum_{i=1}^{r} X_i + X_{+i}} \times 100\% \quad (6)$$

In equations (3) to (6), X_{ii} is the diagonal value of the confusion (error) matrix, and X_{ij} is used for flooded and non-flooded area classifications. The matrix size $r = 2$, X_{i+} is the number of pixels in row i obtained from the remotely sensed analysis, X_{+j} is the number of column j obtained from referenced flood data, and N is the total number of pixels in the sample.

Table 4: Categorization based on a range of kappa coefficient (κ; Watson and Petrie 2010; Sivanpillai et al. 2021).

No.	Coefficient range	Classification
1	$\kappa < 0.00$	Very poor
2	$0 \leq \kappa \leq 0.20$	Poor
3	$0.21 \leq \kappa \leq 0.40$	Fair
4	$0.41 \leq \kappa \leq 0.60$	Moderate
5	$0.61 \leq \kappa \leq 0.80$	Good
6	$\kappa \geq 0.80$	Very good

The kappa coefficient (κ) measures how the classification results compare to values assigned by chance. Furthermore, it is computed from the error matrix and incorporates diagonal and off-diagonal elements (Sivanpillai et al. 2021). Based on the 2015 Indonesian National Institute of Aeronautics and Space guidelines on satellite data processing, the minimum level of accuracy required is 75%. Table 4 shows the range of kappa coefficients and the respective classification.

4 Results

4.1 Flooding extraction

The extraction of flooding for five villages with two approaches (FIEI and MNDWI) and three TVs resulted in thirty images. As an example, in Figure 3, the left column indicates that the MNDWI approach with TV1 treatment overestimated the flooded area. This can be observed especially in several residential or built-up areas.

4.2 Effect of threshold setting

Applying TV treatment is critical to define the flooded and non-flooded areas accurately. Therefore, the application of several TVs to reduce pixel error in flooding extraction is necessary. Figure 4 shows the resulting flood mapping image based on FIEI, where the spatial extent of floods is reduced from TV1 to TV3 when the TV value is raised.

4.3 Accuracy measurement

The measurement results using the overall accuracy method and the kappa coefficients show that the FIEI approach is more accurate than the MNDWI in classifying and mapping flooded and non-flooded areas, as indicated in Table 5. The overall accuracy (OA) of the FIEI approach using three different TVs showed results above 70%, whereby Sanenrejo achieved the highest based on TV1 at 98.04%. Subsequently, the MNDWI approach showed overall accuracy results above 50%, with the TV1 treatment yielding the highest value of 79.69% for Curahnongko.

Table 5: Accuracy assessment for flood maps from the MNDWI and FIEI.

No.	Study area	Threshold value	Overall accuracy (%)		Kappa coefficients	
			FIEI	MNDWI	FIEI	MNDWI
1	Wonoasri	TV1	90.36	75.90	0.83	0.03
		TV2	83.13	64.44	0.54	0.01
		TV3	77.11	70.00	0.43	0.01
2	Curahnongko	TV1	95.24	79.69	0.8	0.17
		TV2	73.44	77.78	0.31	0.10
		TV3	75.81	79.37	0.38	0.12
3	Curahtakir	TV1	94.92	66.10	0.88	0.12
		TV2	77.97	64.41	0.54	0.26
		TV3	74.58	76.27	0.50	0.46
4	Sanenrejo	TV1	98.04	76.47	0.96	0.43
		TV2	90.20	54.90	0.79	0.05
		TV3	80.39	52.83	0.61	0.13
5	Sidodadi	TV1	95.83	79.17	0.86	0.10
		TV2	83.33	62.50	0.57	0.01
		TV3	75.00	58.33	0.44	0.06
Average of TV1			94.88	75.47	0.63	0.14

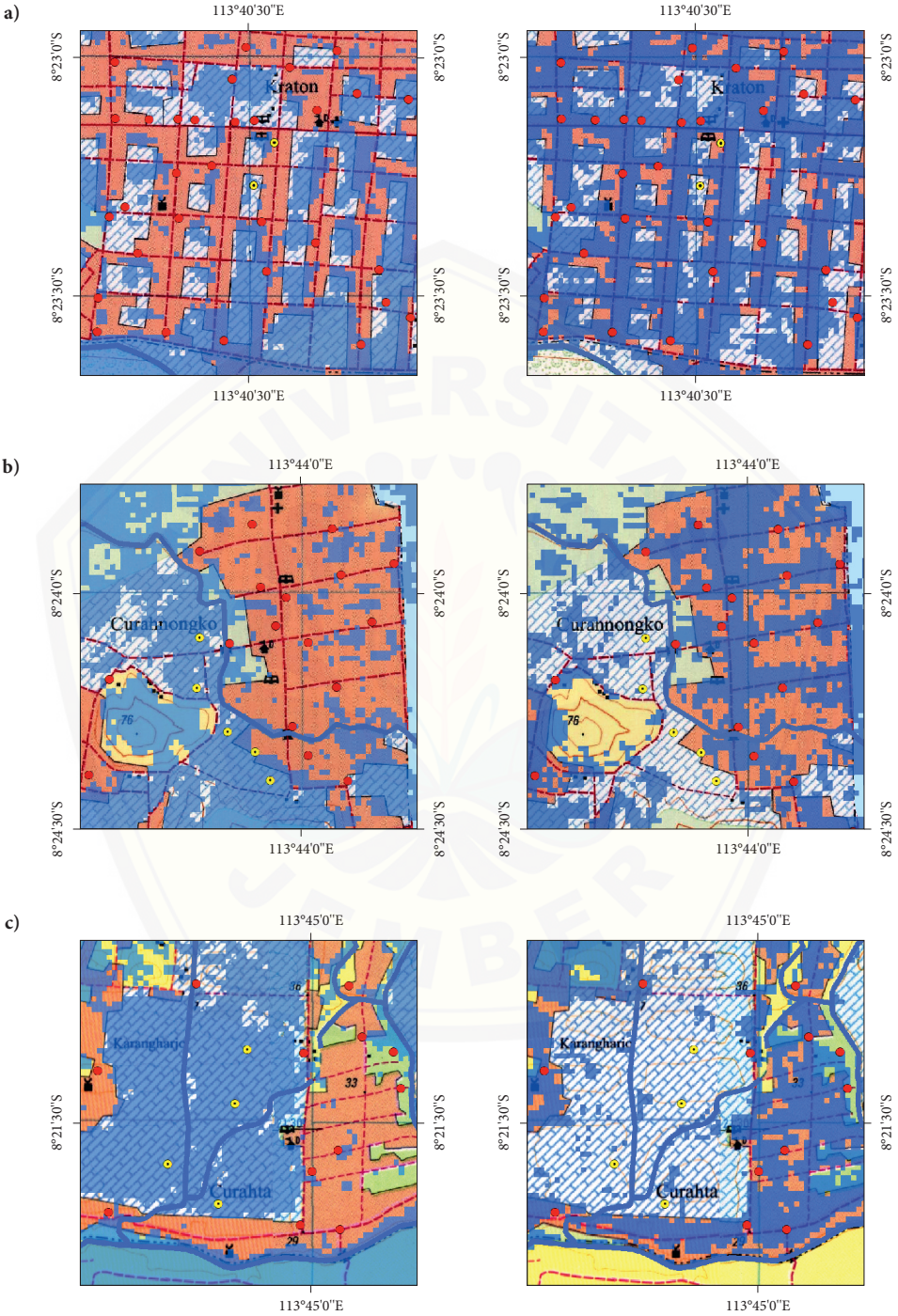

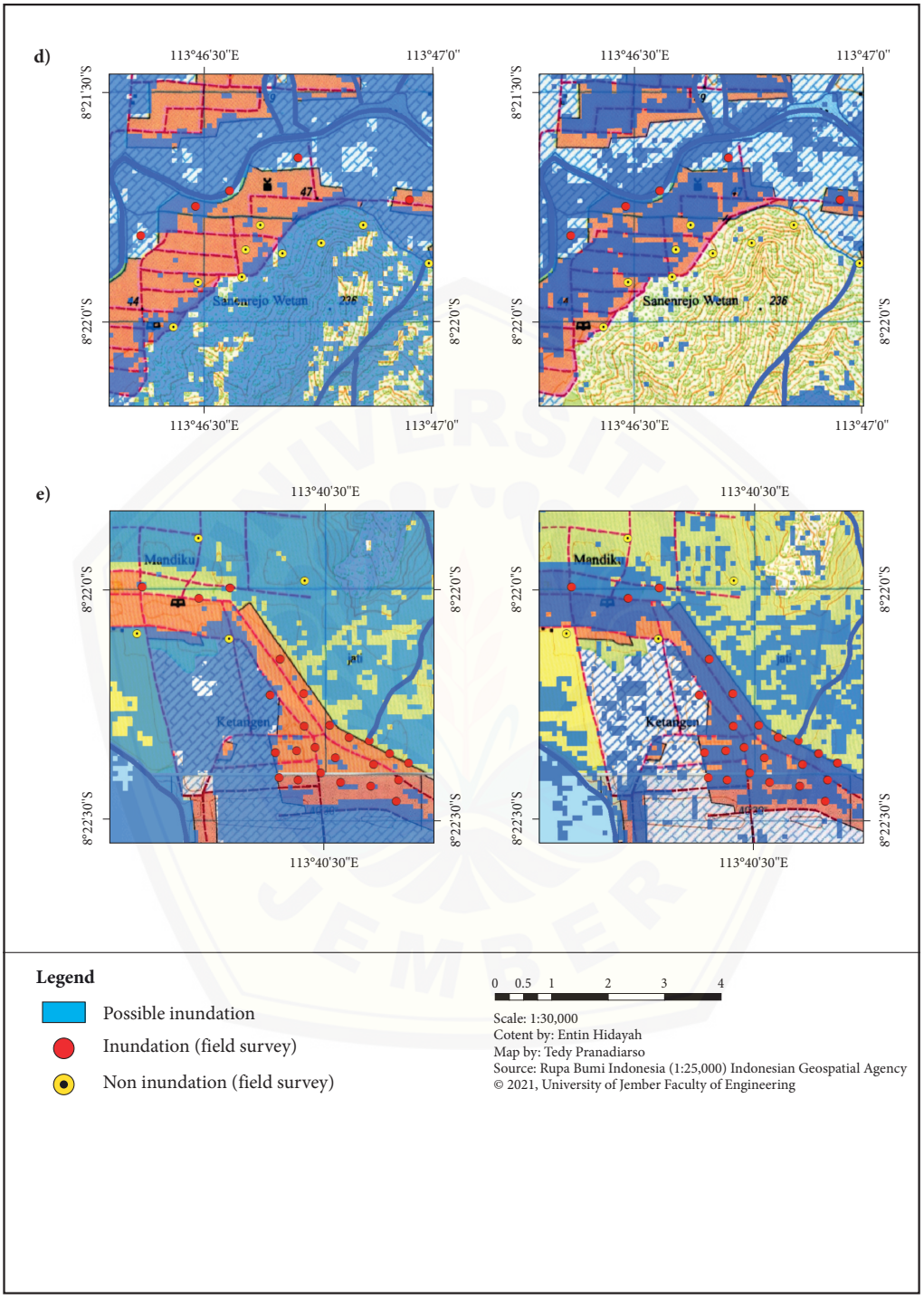

Figure 3: Flooding extraction using MNDWI (left) and FIEI (right) with TV1 for (a) Wonoasri, (b) Curahnongko, (c) Curahtakir, (d) Sanenrejo, and (e) Sidodadi. (p. 56–57)

The kappa coefficients show that the FIEI approach results are more accurate than the MNDWI results. The coefficients of the FIEI approach achieve over 0.8 for the case of TV1 treatment. The highest kappa coefficient of 0.96 is obtained using the FIEI approach in Sanenrejo. Meanwhile, the highest coefficients when using the MNDWI approach are seen in Curahtakir with TV3 treatment. The value of 0.46 obtained

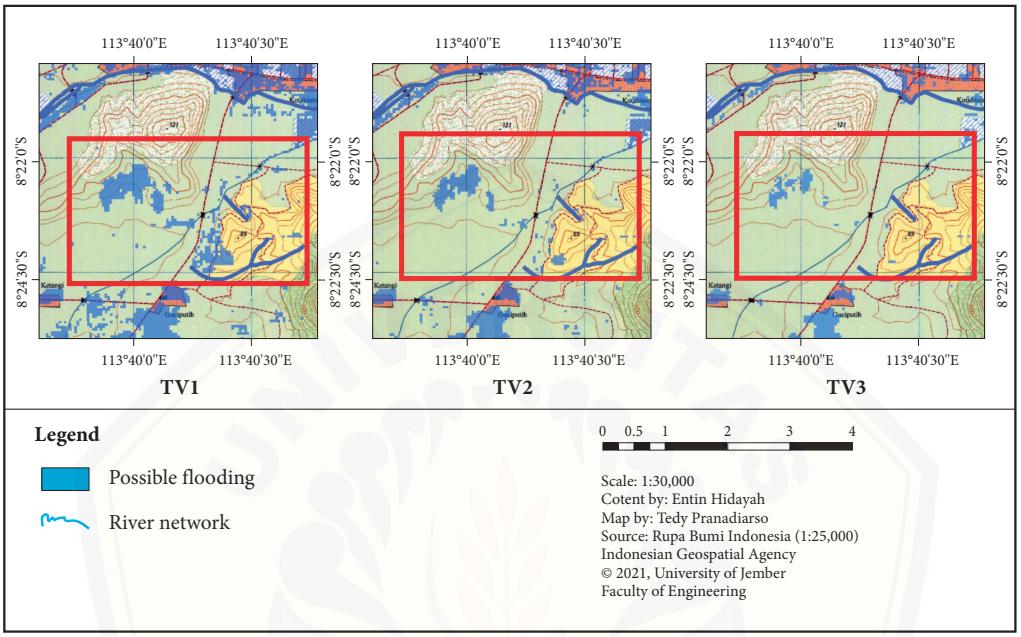

Figure 4: Effect of TV treatment for FIEI.

Table 6: User and producer accuracy assessment for the MNDWI and FIEI approaches.

No.	Study area	Threshold value	User accuracy (%)		Producer accuracy (%)	
			FIEI	MNDWI	FIEI	MNDWI
1	Wonoasri	TV1	91.43	87.14	98.46	84.72
		TV2	81.43	70.13	98.28	85.71
		TV3	74.29	77.92	98.11	85.71
2	Curahnongko	TV1	94.64	87.50	100.00	90.74
		TV2	73.21	83.93	97.62	90.38
		TV3	72.73	85.71	100.00	90.57
3	Curahtakir	TV1	95.12	82.93	97.50	72.34
		TV2	73.17	63.41	93.75	81.25
		TV3	65.85	80.49	96.43	84.62
4	Sanenrejo	TV1	100.00	93.94	97.06	75.61
		TV2	87.88	60.61	96.67	66.67
		TV3	72.73	39.39	96.00	72.22
5	Sidodadi	TV1	95.00	91.67	100.00	84.62
		TV2	80.00	68.33	100.00	83.67
		TV3	70.00	60.00	75.00	85.71

is considered a moderate accuracy. The lower accuracy results obtained by the MNDWI approach are due to the overestimation of flooded areas and misclassifications of flooded and non-flooded regions in residential areas or built-up land use.

The FIEI approach with TV1 treatment can more accurately map flooding in residential (or built-up areas) and vegetation areas than the MNDWI approach. It can produce flooding extraction closer to the actual flood occurrence without overestimation. This is validated by comparing the extracted flooded area with data from a field survey. In some evacuation locations, non-flooded areas are accurately spotted, facilitating evacuation efforts.

For the accuracy of flood maps used by natural disaster emergency response agencies, more detailed validations were needed to evaluate user accuracy (UA) and producer accuracy (PA).

Table 6 shows that the UA and PA values of the FIEI approach were higher than the MNDWI approach. Using the FIEI approach, the UA and PA values were above 90%, reaching 100%. This shows that the classification between flooded and non-flooded areas has been mapped accurately and reliably.

5 Discussion

In East Java Province, from 2017 to 2021, the average flood incidence is 115 events per year. According to the National Disaster Management Agency's data for 2022 showed that 111 people died, two were missing, 10,384 were evacuated, and 1,599 buildings were damaged (https://gis.bnpb.go.id/). Flood mapping is very expensive and takes a long time, hence the flood mapping technique with the Sentinel-2 image approach is needed for mitigation efforts (Sivanpillai et al. 2021).

Previously, the NDWI and MNDWI algorithms were applied based on Landsat, Sentinel-1, and Sentinel-2 images for rapid flood mapping with various features for water bodies and flooded areas. In Shouguang, both algorithms based on Sentinel-1 and Sentinel-2 with random forest classification for rivers showed OA values of 85.22% and 95.45%, respectively (Huang and Jin 2020). Furthermore, for rural watershed areas in Australia, using two algorithms based on Landsat Oli 8 imagery with unsupervised classification proved to be effective, with OA values of 96.04% and 95.70%, respectively (Ghofrani et al. 2019). Implementation on rivers and lakes in Canada, the Tennessee River in the US, the Swedish lake Lungsjön, and Mongolia's Lake Khar-Us using Sentinel-2 imagery showed outstanding accuracy with consecutive OA values based on the NDWI (0.97, 0.965, 0.94, and 0.925) and the MNDWI (0.97, 0.962, 0.96, and 0.945; Niu et al. 2022). The application of the Landsat image–based MNDWI to features of urban land, rural land, vacant land, swamps, and agricultural areas in the US had an overall accuracy of 93.92% (Sivanpillai et al. 2021). In addition, the MNDWI algorithm application based on the Landsat image for the same feature also yielded excellent results, as shown in Table 7 (Feyisa et al. 2014). The application of the MNDWI for coastal forests, agriculture, grasslands, shrubs, and forests in eastern Australia using Landsat imagery also resulted in outstanding accuracy, with an OA value of 97.95% (Fisher et al. 2016). Implementation of the NDWI and

Table 7: Implementation of MNDWI in several countries.

Location	Accuracy (%)	TV	Land use	Reference	Data sources
Denmark	98.05 (UA)	0.1	Reservoirs, a harbor, and the sea (Øresund and Køge Bay)	Feyisa et al. 2014	Landsat
Switzerland	99.84 (UA)	−0.15	Lake Lauerz, Lake Ägeri, Lake Sihl, Lake Wägital, Lake Klöntal	Feyisa et al. 2014	Landsat
Ethiopia	96.60 (UA)	0.1	Gefersa, Dire, Legedadi	Feyisa et al. 2014	Landsat
South Africa	94.46 (UA)	0.6	Berg River, Wemmershoek, Brandvlei	Feyisa et al. 2014	Landsat
New Zealand	98.14 (UA)	0.2	Lake Te Anau	Feyisa et al. 2014	Landsat
Eastern Australia	97.95 (OA)	0.1	Coastal forest, agricultural, grasslands, shrublands, woodlands	Fisher et al. 2016	Landsat
US	93.92 (OA)	0.2	Urban, rural, bare ground, marshes, agricultural area	Sivanpillai et al. 2021	Landsat
China	85.22 (OA)	0.35	Several rivers	Huang and Jin 2020	Sentinel-2
Spain	68 (OA)	−0.35	Wetlands	Pena-Regueiro et al. 2020	Sentinel-2

Note: UA = user accuracy, OA = overall accuracy.

MNDWI for rivers and lakes yielded excellent results. However, its implementation based on Sentinel-2 for coastal areas in Valencia in eastern Spain resulted a decrease in performance, as indicated by OA values of 89% and 68% (Pena-Regueiro et al. 2020). Similarly, in our research the application of the MNDWI for lowland flooding is also unsatisfactory, with an average OA value of 75.47% (Table 6). It is important to emphasize that the MNDWI has weaknesses in detecting the water layer underlying the built-up area in lowlands and also in the coastal area.

Therefore, with outstanding results, we are using the FIEI algorithm to develop rapid flood mapping using Sentinel-2 imagery and changing the band combination in lowland flooding. The performance of the FIEI approach provides an average increase in the overall accuracy of 19.41% from the MNDWI in consistent flood mapping for five villages in the Tempurejo sub-district, Jember Regency, Indonesia. The increased average of overall accuracy (19.41%) is obtained by calculating the mean of the overall accuracy of FIEI's TV1 minus the mean of the overall accuracy of MNDWI's TV1. As a highlight, the FIEI is an improvement from the MNDWI for lowland flooding by utilizing NIR waves sensitive to water that can capture lowland flooding. Meanwhile, the MNDWI application with the most optimal TV equaling 0 cannot provide better accuracy.

In addition to the combination of bands, the TV is also influential in achieving the best accuracy. Each country had a different TV for achieving the best accuracy, as shown in Table 7. Some locations had the same TV, equal to 0.1, such as Denmark, Ethiopia, and eastern Australia (Feyisa et al. 2014; Fisher et al. 2016). In addition, New Zealand and the US have the same TV score, at 0.2. In other countries, the best accuracy was obtained from a TV less than 0 (Feyisa et al. 2014; Sivanpillai et al. 2021; Xu 2006; Pena-Regueiro et al. 2020). Whereas this study shows that using an appropriate TV1 greater than or equal to 0 is flooding, the flooding extraction eliminates falsely classified pixels. In our study case, selecting the proper TV is expected to produce more optimal map accuracy.

The FIEI approach with treatment TV1 can effectively provide crucial and timely information on flooded areas to map out priority evacuation areas affected by disasters. This saves time in allocating resources to places that require evacuation to facilitate the distribution of logistical assistance. In line with Kaplan and Avdan's (2017) opinion, remote sensing techniques are often less costly and time-consuming for large geographic areas than conventional field mapping. The FIEI algorithm using Sentinel-2 imagery can be applied for rapid mapping of floods in other countries. This map is classified into flooded and non-flooded areas suitable for lowland applications and beneficial in planning flood mitigation. This flood map is certainly very useful in mapping flood risk (Ryu et al. 2017), planning flood mitigation (Sipelgas et al. 2021), or managing small retention ponds (Ferk et al. 2020).

6 Conclusion

The FIEI approach addressed the MNDWI's limitations and prevented overestimation of the flooded area. Compared to the MNDWI approach, it analyzes bands 3, 8, and 11 of Sentinel-2 to extract flooded areas more effectively. Furthermore, it provides higher accuracy with the appropriate TV treatment. The approach is recommended for quickly mapping flooded areas (if ground truth data are available) in the Tempurejo sub-district and similar lowland areas susceptible to flooding.

With free spatial data and ground truth data, the FIEI approach is suitable for deployment during disasters to provide quick flood mapping for response, evacuation, and mitigation efforts. The technique can be easily extended to other locations if the TV is successfully identified. For applying flood mapping outside Indonesia, such as in Denmark, Australia, China, New Zealand, and the US, a combination of bands 3 and 12 is recommended.

ACKNOWLEDGMENTS: This article is part of a research program supported by funding from the Indonesia Endowment Fund for Education (LPDP) in 2021–2022.

7 References

Bousbih, S., Zribi, M., Pelletier, C., Gorrab, A., Lili-Chabaane, Z., Baghdadi, N., Ben Aissa, N., Mougenot, B. 2019: Soil texture estimation using radar and optical data from Sentinel-1 and Sentinel-2. Remote Sensing 11-13. DOI: https://doi.org/10.3390/rs11131520

Chen, Z., Luo, J., Chen, N., Xu, R., Shen, G. 2019: RFim: A real-time inundation extent model for large floodplains based on remote sensing big data and water level observations. Remote Sensing 11-13. DOI: https://doi.org/10.3390/rs11131585

Ettehadi Osgouei, P., Kaya, S., Sertel, E., Alganci, U. 2019: Separating built-up areas from bare land in Mediterranean cities using Sentinel-2A imagery. Remote Sensing 11-3. DOI: https://doi.org/10.3390/rs11030345

European space agency 2015: Sentinel-2 user handbook. European Space Agency Standard Document 1-2.

Ferk, M., Ciglič, R., Komac, B., Lóczy, D. 2021: Management of small retention ponds and their impact on flood hazard prevention in the Slovenske Gorice Hills. Acta geographica Slovenica 61-1. DOI: https://doi.org/https://doi.org/10.3986/AGS.7675

Feyisa, G. L., Meilby, H., Fensholt, R., Proud, S. R. 2014: Automated Water Extraction Index: A new technique for surface water mapping using Landsat imagery. Remote Sensing of Environment 140. DOI: https://doi.org/10.1016/j.rse.2013.08.029

Fisher, A., Flood, N., Danaher, T. 2016: Comparing Landsat water index methods for automated water classification in eastern Australia. Remote Sensing of Environment 175. DOI: https://doi.org/10.1016/j.rse.2015.12.055

Gašparovič, M., Klobučar, D. 2021: Mapping floods in low-land forest using Sentinel-1 and Sentinel-2 data and an object-based approach. Forests 12-5. DOI: https://doi.org/10.3390/f12050553

Ghofrani, Z., Sposito, V., Faggian, R. 2019: Improving flood monitoring in rural areas using remote sensing. Water Practice and Technology 14-1. DOI: https://doi.org/10.2166/wpt.2018.118

Huang, M., Jin, S. 2020: Rapid flood mapping and evaluation with a supervised classifier and change detection in Shouguang using Sentinel-1 SAR and Sentinel-2 optical data. Remote Sensing 12-13. DOI: https://doi.org/10.3390/rs12132073

Kaplan, G., Avdan, U. 2017: Mapping and monitoring wetlands using Sentinel-2 satellite imagery. ISPRS Annals of the Photogrammetry, Remote Sensing and Spatial Information Sciences IV-4/W4. DOI: https://doi.org/10.5194/isprs-annals-IV-4-W4-271-2017

Mahmood, S., Sajjad, A., Rahman, A.-ur. 2021: Cause and damage analysis of 2010 flood disaster in district Muzaffar Garh, Pakistan. Natural Hazards 107. DOI: https://doi.org/10.1007/s11069-021-04652-6

Niu, L., Kaufmann, H., Xu, G., Zhang, G., Ji, C., He, Y. 2022: Triangle Water Index (TWI): An advanced approach for more accurate detection and delineation of water surfaces in Sentinel-2 data. Remote Sensing 14-21. DOI: https://doi.org/https://doi.org/10.3390/rs14215289

Niwas, R., Grewal, M. S., Khichar, M. L. 2015: Practical manual on Remote Sensing , GIS and Land Use Planning. Hisar.

Nurullatifah, T. 2021: Ribuan Warga Terdampak Banjir di Jember. Internet: https://akurat.co/ribuan-warga-terdampak-banjir-di-jember (25. 1. 2023).

Pena-Regueiro, J., Sebastiá-Frasquet, M.-T., Estornell, J., Aguilar-Maldonado, J. A. 2020: Sentinel-2 application to the surface characterization of small water bodies in wetlands. Water 12-5. DOI: https://doi.org/10.3390/w12051487

Rahman, M., Ningsheng, C., Islam, M. M., Dewan, A., Iqbal, J., Washakh, R. M. A., Shufeng, T. 2019: Flood susceptibility assessment in Bangladesh Using machine learning and multi-criteria decision analysis. Earth Systems and Environment 3. DOI: https://doi.org/10.1007/s41748-019-00123-y

Ryu, J., Yoon, E. J., Park, C., Lee, D. K., Jeon, S. W. 2017: A flood risk assessment model for companies and criteria for governmental decision-making to minimize hazards. Sustainability 9-11. DOI: https://doi.org/10.3390/su9112005

Sajjad, A., Lu, J., Chen, X., Chisenga, C., Mazhar, N., Nadeem, B. 2022: Riverine flood mapping and impact assessment using remote sensing technique: A case study of Chenab flood-2014 in Multan district, Punjab, Pakistan. Natural Hazards 110. DOI: https://doi.org/https://doi.org/10.1007/s11069-021-05033-9

Sarp, G., Ozcelik, M. 2017: Water body extraction and change detection using time series: A case study of Lake Burdur, Turkey. Journal of Taibah University for Science 11-3. DOI: https://doi.org/10.1016/j.jtusci.2016.04.005

Sathianarayanan, M. 2018: Assessment of surface water dynamics using multiple water indices around Adama woreda, Ethiopia. ISPRS Annals of the Photogrammetry, Remote Sensing and Spatial Information Sciences 4-5. DOI: https://doi.org/10.5194/isprs-annals-IV-5-181-2018

Sipelgas, L., Aavaste, A., Uiboupin, R. 2021: Mapping flood extent and frequency from Sentinel-1 imagery during the extremely warm winter of 2020 in boreal floodplains and forests. Remote Sensing 13-23. DOI: https://doi.org/10.3390/rs13234949

Sivanpillai, R., Jacobs, K. M., Mattilio, C. M., Piskorski, E. V. 2021: Rapid flood inundation mapping by differencing water indices from pre- and post-flood Landsat images. Frontiers of Earth Science 15. DOI: https://doi.org/10.1007/s11707-020-0818-0

Suwarsono, Nugroho, J. T., Wiweka. 2013: Identification of inundated area using normalized difference water index (NDWI) on lowland region of Java island. International Journal of Remote Sensing and Earth Sciences 10-2. DOI: https://doi.org/10.30536/j.ijreses.2013.v10.a1850

Wang, Y., Colby, J. D., Mulcahy, K. A. 2002: An efficient method for mapping flood extent in a coastal floodplain using Landsat TM and DEM data. International Journal of Remote Sensing 23-18. DOI: https://doi.org/10.1080/01431160110114484

Watson, P. F., Petrie, A. 2010: Method agreement analysis: A review of correct methodology. Theriogenology 73-9. DOI: https://doi.org/10.1016/j.theriogenology.2010.01.003

Xu, H. 2006: Modification of normalized difference water index (NDWI) to enhance open water features in remotely sensed imagery. International Journal of Remote Sensing 27-14. DOI: https://doi.org/10.1080/01431160600589179

Zhou, Y., Dong, J., Xiao, X., Xiao, T., Yang, Z., Zhao, G., Zou, Z., Qin, Y. 2017: Open surface water mapping algorithms: A comparison of water-related spectral indices and sensors. Water 9-4. DOI: https://doi.org/10.3390/w9040256Bousbih, S., Zribi, M., Pelletier, C., Gorrab, A., Lili-Chabaane, Z., Baghdadi, N., Aissa, N. Ben., Mougenot, B. 2019: Soil texture estimation using radar and optical data from Sentinel-1 and Sentinel-2. Remote Sensing. DOI: https://doi.org/10.3390/rs11131520